Research Article

For reprint orders, please contact: reprints@futuremedicine.com

Nanomedicine

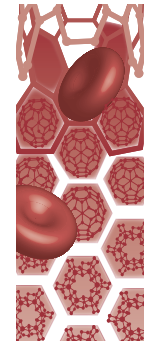

Electrochemical nanostructured ZnO biosensor for ultrasensitive detection of cardiac troponin-T

Aim: Vertically oriented zinc oxide nanostructures based disposable diagnostic biosensor for detecting and quantifying levels of cardiac troponin-T from human serum has been developed. **Materials & methods:** The biosensors were designed by integrating hydrothermally grown zinc oxide nanostructures on glass and printed circuit board platforms, resulting in the generation of high-density nanostructure arrays with nanotextured zinc oxide based electrodes. The size, density and surface terminations of the nanostructures were leveraged toward achieving surface confinement of the target cTnT molecules on to the nanostructures. A combination of AC and DC spectroscopy was used to characterize the biosensor response to cTnT. **Results & conclusion:** LOD of 0.1 pg/ml in human serum was achieved.

First draft submitted: 11 February 2016; Accepted for publication: 12 April 2016; Published online: 19 May 2016

Keywords: cardiac troponin-T • electrochemical impedance spectroscopy • label-free biosensor • Mott–Schottky • zinc oxide nano electrodes

Nandhinee Radha Shanmugam[‡,1], Sriram Muthukumar[‡,2], Anjan Panneer Selvam[1] & Shalini Prasad*[,1]

[1]Department of Bioengineering, University of Texas at Dallas, Richardson, TX 75080, USA

[2]Enlisense LLC, 1813 Audubon Pond Way, Allen, TX 75013, USA

*Author for correspondence: shalini.prasad@utdallas.edu

[‡]Authors contributed equally

Cardiovascular diseases (CVDs) has highest mortality risk in the USA and Europe with 15–20 million cases being reported annually [1]. Among CVDs, acute myocardial infarction (AMI) has the highest mortality within hours of onset and hence is the most life threatening [2]. Thus, early diagnosis is necessary to save patient's life. AMI is characterized by prolonged ischemic necrosis of cardiac myocytes that affects the myocardial cellular repair mechanisms resulting in irreversible cell damage or death [3,4]. Current means of AMI diagnosis include observations through electrocardiograms (ECGs) and measurement of cardiac specific biomarker levels in blood [4]. ECGs of suspected AMI patients are often normal and ambiguous, leading to misdiagnosis [5]. As a result, cardiac biomarkers are now used in the diagnosis and risk stratification of patients with chest pain and suspected acute coronary syndrome (ACS) [1]. Thus, measurement of its levels is critical to make accurate interventions and early triage of patients at risk [6].

Proteins namely; c-reactive protein, myoglobin and troponins are the three main biomarkers released into bloodstream when heart muscles degenerate [4,7]. The concentrations of these proteins reflect the pathophysiological condition of patient [6]. Recent studies have shown cardiac troponin-T (cTnT) and troponin-I (cTnI) to be more sensitive and specific for myocardial cell damage and hence considered as 'gold standard' and central to AMI diagnosis [4,8]. Troponins have half-life of about 2 h and upon onset of AMI, their levels are elevated within 4 h and persist in the blood for 4–10 days [9,10]. Currently, quantitative determination of cardiac troponins is performed through label-based assays, which are complex, expensive, laborious and time-consuming [11]. Further, use of labels alters the physical characteristics of biomolecules [12]. Table 1 illustrates the list of commercially available label-based diagnostic assays for cardiac troponins [9,11,13]. Label-free electrochemical techniques (which includes amperometry,

Future Medicine part of fsg

Table 1. High-sensitivity troponin diagnostic label-based assays commonly used in current clinical practices.

Commercially available troponin assays	99th percentile cut-off (ng/ml)
cTnT	
Roche Elecsys, third generation	0.01
cTnI	
Abbott AxSYM	0.30
Bayer ACS: Centaur	0.15
Bayer ACS: 180	0.07
Beckman Access, second generation	0.04
DPC Immulite	0.40
Abbott Architect	0.04
Siemens: Dimension Vista	0.05

potentiometry, conductometry etc.) has potential advantages of simplicity, detection in real time, robustness and has prospect of developing into hand-held devices for point-of-care (PoC) applications [2]. Among these techniques, electrochemical impedance spectroscopy (EIS) is widely used to measure the charge perturbations at the electrode surface occurring due to conjugation between the capture probe and target molecule [14]. These physicochemical interactions can be converted into measurable electrical signals. However, these electrical signals are very weak, hence signal amplification is required to enhance the sensitivity of detection. Modification of electrode surfaces with nanomaterials increases the surface area for capture probe immobilization and target biomolecule interaction [7,15]. Nanostructured electrode surfaces have shown to improve the sensitivity and detection limit of target biomolecules [16,17].

The ability to create nanostructures with desired chemical and electrical properties at the nanoscale and to integrate them into high-density arrays toward designing functional and tuneable devices has sparked significant interest in the use of semiconducting metal oxides [18]. Nowadays, metal oxide nanostructures are utilized for wide ranging applications from nanoelectronics to nanomedicine [19]. Zinc oxide (ZnO) is attractive and extensively studied metal oxide semiconductor due to its multifunctional properties such as wide direct band gap (3.37 eV), large exciton binding energy (60 meV), nontoxicity, chemical stability, ionic bonding, biocompatibility, etc. [20,21]. Metal oxide based nanomaterials with high isoelectric point (IEP) such as ZnO have been found to be suitable for the immobilization of low IEP biomolecules [17]. These properties have extended its use in designing gas sensors [22], thin film transistors [18,20] and bio-chemical detection [23,24]. The high ionic strength offers strong and stable interactions with biomolecules under physiological pH that is important characteristics for designing biosensing and biomedical applications.

ZnO is also naturally n-type semiconductor with polar and nonpolar surfaces along the primary c-axis growth plane that allows for synthesis of highly ordered and oriented nanostructures using both gas and liquid phase synthesis methods [18,21,25]. Electrical conductivity in 1D nanostructures is a complex transport phenomenon dependent on size effects and surface states [26]. The placement of atoms along the crystal planes in a 1D nanostructure can be preferentially modulated to enhance direct and fast electron/charge transport on the surface in electrolyte solutions. These phenomena enhanced at the surface of the 1D nanostructures along with maximized surface area to volume can be leveraged to amplify the electrical detection thus enhancing sensitivity in biosensing [27]. Highly specific binding is thus achieved through selective surface chemistry techniques applied to 1D nanostructures. ZnO nanostructures is one such platform that can help in electrical transduction of biomolecular interaction from biomolecules [23,28,29] (e.g., proteins, DNA, RNA, etc.) into amplified signal response. The high electron transfer kinetics of 1D ZnO nanostructure also allows for detection of biomolecules with enhanced sensitivity and selectivity. The surface-charges and electrical transport properties of these 1D nanostructured ZnO biosensor platform are modulated by the highly ordered crystalline orientation of the nanostructures [25], uniformity in height and density all of which can be easily tuned with solution-based synthesis methods. Hence, simple, robust, label-free and low-cost portable electrical biosensors can be designed by integration of 1D ZnO nanostructure electrodes in electrochemical biosensing devices. We have previously demonstrated the use of nanotextured zinc oxide thin films on printed circuit board electrodes to detect cTnT. In our previous work, we reported challenges in achieving ultra-sensitivity and specificity due to the inability to distinguish between the semiconductor capacitance offered by ZnO vis-à-vis the double layer capacitance changes associated with the biomolecule binding [30]. Hence, in this work we have addressed these challenges through a novel nanoelectrode design comprising of ZnO nanostructures that enhances the double layer and implementation of a combinatorial electrochemical analysis methods toward identifying biomolecule mediated capacitance changes.

Here, we report the development of 1D electrically tunable nanostructured ZnO biosensor platform for ultra-sensitive and highly specific detection of cTnT. The nanostructured electrodes offer enhanced signal response due to biomolecule confinement [28]; and enhanced sensitivity due to the ionic and semiconducting nature of ZnO. The biomolecular interactions occur-

ring at the surface of nanostructured ZnO results in formation of electrical double layer (EDL) at ZnO electrode–electrolyte interface [31]. The ZnO surface states strongly impact electro-ionic charge-transfer dynamics in the EDL and hence the electrochemical behavior is predominant at the 1D ZnO nanostructured electrodes than its bulk counterparts [32]. As a result, 1D ZnO nanostructured sensor surfaces enable faster reaction kinetics and increased S/N leading to enhanced sensitivity of detection. The interactions modulating the dynamic charge transport in 1D ZnO nanostructures are characterized as resistive and capacitive changes through EIS measurements. The binding of biomolecules to 1D ZnO nanostructures also modulates the localized charge distribution at the electrode–electrolyte interface, resulting in work-function modulation of the semiconducting ZnO that can be characterized as space-charge capacitance (C_{sc}) changes through Mott–Schottky measurements. Therefore, the same interactions that causes a change to the EDL is expected to also cause a change to the space-charge capacitance. We present both these novel methods of characterizing the modulations to EDL and space-charge regions along 1D ZnO nanostructured interfaces to determine their efficacy in electrochemical detection of cTnT.

Materials & methods

Chemicals & reagents

Zinc nitrate hexahydrate ($Zn(NO_3)_2.6H_2O$), hexamethylenetetramine (HMTA), phosphate buffered saline (PBS) and Superblock were purchased from Thermo Scientific. Deionized (DI) water, DMSO, human serum (HS), polydimethylsiloxane and cross-linker (dithiobis(succinimidyl propionate)) (DSP) were all obtained from Fisher Scientific. Bovine serum albumin (BSA) were obtained from Sigma Aldrich. Anti-cTnT monoclonal antibody and cTnT antigen were obtained from US Biological. All other chemicals used were of reagent grade and was used without any further purification.

Preparation of ZnO seeded substrates

Silicon wafer, gold microelectrode (two planar electrodes) patterned FR4 and glass slides were used as substrates for nanostructures growth. The substrates were cleaned in an ultrasonic bath with acetone, isopropyl alcohol and DI water in consecutive manner each for a minute to remove any surface bound impurities and dried under nitrogen prior to use. The substrates were then placed in RF magnetron sputtering chamber to selectively deposit ZnO seed layer on the microelectrodes. The deposition parameters (140 W power, absence of oxygen plasma, 15mTorr pressure) were obtained from our previous work [33]. The ZnO seed acts as nucleation sites and thus the uniformity and thickness of seed layer was determined by profilometer measurements.

Synthesis of ZnO nanostructured electrodes

ZnO nanostructures were grown in aqueous chemical bath at temperature much lower than the boiling point of water. The aqueous growth solution was prepared by dissolving equimolar concentration (1:1 ratio) of ($Zn(NO_3)_2.6H_2O$) and HMTA in 500 ml DI water. The seeded substrate was suspended upside down in solution and reaction between precursors was allowed to proceed for 30 min duration. The growth temperature and spin speed was maintained at 80°C and 100 rpm respectively. Finally, the substrates were rinsed in DI water and dried in air. Precursor concentrations of 25, 50, 75 and 100 mM were investigated to study its influence on growth and hence the sensitivity of biomolecules detection.

Surface modification of ZnO nanostructured electrodes

First, the nanostructured electrode surface is treated with 10 mM DSP dissolved in DMSO for an hour. The disulfide bond in its 12-spacer arm interacts with Zn^+ sites through thiol conjugation. Then, linker functionalized sensor surface was incubated for 30 min with 1 µg/ml of anti-cTnT in PBS. The N-hydroxysuccinimide (NHS) group at the terminal ends of linker reacts with amine groups present in monoclonal antibody forming a strong covalent amide linkage. The exposed NHS sites of DSP molecules were then blocked with Superblock for 30 min to eliminate chances for nonspecific interactions. Then, aliquots of cTnT antigen in PBS or HS, starting with lowest concentration is tested on sensor surface each with incubation for 20 min. The excess molecules at each step is removed by washing the sensor surface three-times with suitable buffer medium. The sample volume was maintained at 50 µl. A schematic representation is illustrated in Supplementary Figure 1.

Electrochemical measurements

The electrochemical biosensor platform comprises of an ensemble of ZnO nanoelectrodes grown on metal microelectrode with electrical readouts. The working, counter and reference electrodes were nanostructured ZnO, planar gold and Cu, respectively. The electrochemical measurements are taken at each step of immunoassay using Gamry reference 600 potentiostat. Each measurement is taken in three cycles to ensure measurements at steady-state conditions and reproducibility. The change in output signal response before and after antigen interaction is used to build

calibration curve. A polydimethylsiloxane microfluidic encapsulant bonded to sensor platform is used to hold the sample on the sensing region.

Results

Morphology of ZnO nanostructured sensing surface

The morphology of ZnO nanostructured surface was studied using scanning electron microscopy (SEM; Zeiss). Figure 1 shows the SEM micrograph of the 1D ZnO nanostructures synthesized via solution route with varying precursor concentration (10, 25, 50, 75 and 100 mM). The growth mechanism, parameters and their influence on nanostructures formation [34–36] are listed in the Supplementary Information.

Figure 1 shows that the density of ZnO nanostructures is modulated by precursor concentration. In general there was a direct correlation between precursor concentration in the range from 10 to 75 mM and density of the ZnO nanostructures indicating a nucleation controlled process. For a growth duration of 30 min, 10 mM precursor concentration yielded extremely sparse growth on seed while ZnO nanostructures with 'rod' shaped morphologies, average length of 400 nm and sub-100 nm diameters were achieved with precursor concentrations of 25, 50 and 75 mM, respectively. Densely packed growth (similar to a thin film) was obtained for 100 mM precursor concentration. The optimal precursor growth concentration for electrochemical biosensing was established through electrode robustness studies conducted with I–V hysteresis and cyclic voltammetry as described in the following section.

Investigation of ZnO nanostructured electrode behavior

The electrical properties of as-grown 1D ZnO nanostructures were characterized by measuring the hysteretic I–V characteristics between 0.01 and 0.1 V in different buffer solutions (DI water, PBS, Tris, HS and synthetic sweat) on all growth samples. The electrochemical biosensor surface exhibits hysteresis behavior due to diffusion of mobile ions in the electrolyte and adsorption onto the nanoelectrode surfaces. As a result, slope and hysteresis changes depending on the ionicity of the buffer solution (shown in Supplementary Figure 2). PBS and HS which have similar conductivity and pH show similar I–V characteristics. Figure 2B shows the response observed for PBS buffer and width of hysteresis loop with increasing precursor concentration. Seed and 10 mM precursor growth display identical I–V characteristics while, the ideal I–V characteristics is observed for 50 and 75 mM precursor concentrations. These experimental results indicate the ability to modulate charge transfer on 1D ZnO nanostructures surfaces which are relevant and critical for designing a biosensor based on electrochemical transduction.

The 'rod' like 1D ZnO nanostructures facilitates the semi-infinite hemispherical diffusion of molecules to the electrode-electrolyte interface, in other words, diffusion profile of the ions and biomolecules is radial to the nanostructure surface as shown in Figure 2A. As a result, each ZnO nanostructure behaves as a nanoelectrode that has faster reaction kinetics, which facilitates physiological fluid measurements at steady state conditions as opposed to microelectrode and planar platforms. This phenomenon of radial diffusion was investigated using cyclic voltammetry. Cyclic voltammetry experiments were performed in 1:1 mixture of PBS and 0.1 M potassium ferrocyanide solution between -1 V and 1 V at a scan rate of 20 mV/s. Figure 2C shows the cyclic voltammograms observed on ZnO seed and nanostructured (50 mM) electrode surface. The charge densities calculated from the area under the curve are 8.995 $\mu C/cm^2$ and 68.64 $\mu C/cm^2$ for seed and 50 mM nanostructured electrode surface respectively. The spacing between nanoelectrodes with 50 mM growth was estimated to be approximately 3× more than that with 100 mM growth and as expected the effective charge density measured on 50 mM electrode surface was much higher than 100 mM (19.241 $\mu C/cm^2$) electrode surface.

EIS measurements were done for further validation of voltammetry results of ZnO nanostructured electrode/electrolyte characteristics. The electrical impedance response was measured by applying a sinusoidal voltage signal of 10 mV over frequencies ranging from 100 to 1 MHz. Nyquist plots of real impedance versus the imaginary impedance are shown in Figure 2D for nanoelectrode surface functionalized with DSP linker. Two semicircular arcs, one each at low- and high-frequency regions were observed. This suggests the presence of two relaxation time constants: one inherent to ZnO surface and other to the charge perturbations in EDL. A decrease in charge transfer resistance (R_{ct}) and increase in double layer capacitance (C_{dl}) with increasing precursor concentrations of growth demonstrated the nanostructure surface coverage as a key factor in determining the electrochemical impedance response. Different characteristics in the impedance spectra were observed for varying precursor concentrations. Both seed and 100 mM nanostructured surface exhibited a semicircular impedance spectra whereas 75 mM surface exhibited a straight line. A semicircular impedance is indicative of the resistive behavior of the electro-ionic charge transfer and a straight line is indicative of diffusion-limited process in which Z_w (Warburg element) in

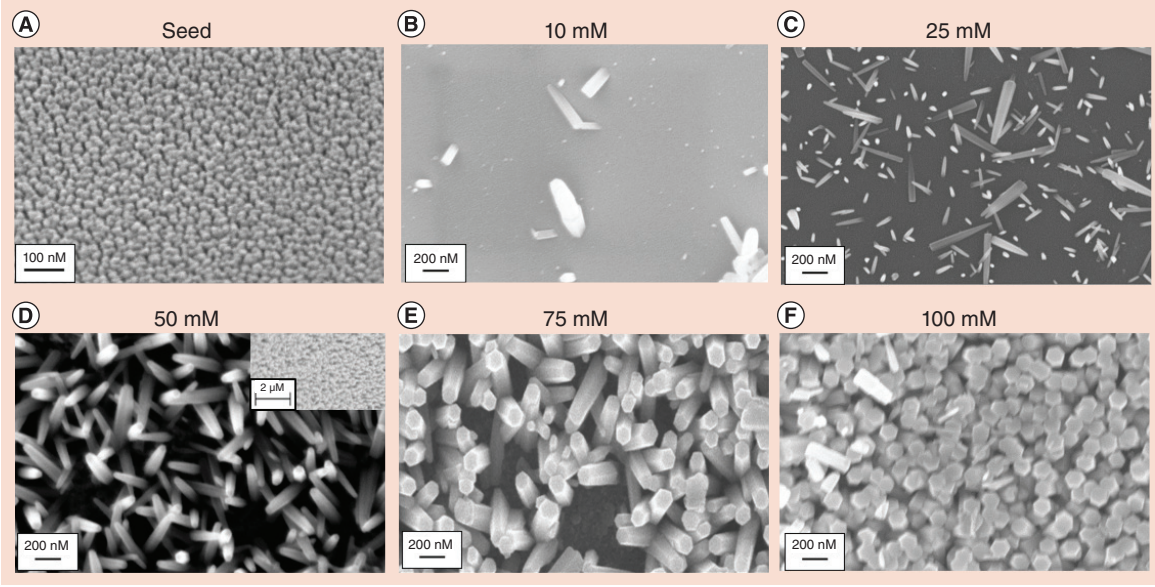

Figure 1. SEM characterization of ZnO nanostructures synthesized via chemical route on RF-magnetron sputtered seed substrate. (A) ZnO seed deposited at 140 W power for 10 min with 15 mTorr pressure in absence of oxygen; **(B–F)** ZnO nanostructures grown hydrothermally on ZnO seed with varying precursor concentration for 30 min.

the Randle's equivalent circuit [14] becomes the dominant component. The Warburg element has both resistive and capacitive features which can be considered as parasitic elements and contribute to the noise in the system. In contrast, both 25 and 50 mM nanostructured surface exhibited two incomplete semicircular arcs with negligible Z_w illustrating that major contribution to electrochemical response comes from charge-transfer controlled process that is capacitive in nature and primarily occurring at low frequencies (below 1 kHz), which again is indicative of charge storage within EDL. Such nanoelectrodes-based electrochemical biosensor platforms offers signal amplification and high S/N required for ultrasensitive detection of biomolecules. Hence, 50 mM growth concentration was selected as an optimal concentration to design nanoelectrode electrochemical biosensor for detection of cTnT.

Electrochemical characterization of ZnO nanoelectrode/electrolyte interface

Response to protein interactions at EDL formed at the electrolyte interface

Figure 3 shows Nyquist and Bode plots observed on nanoelectrode electrochemical biosensor for cTnT antigen concentrations between 0.001 and 100,000 pg/ml. Changes in magnitude and phase of the measured output impedance response were used to characterize the protein biomolecules binding events. cTnT antigen was injected into α-cTnT immobilized nanoelectrodes starting with lowest concentration (0.001 pg/ml of cTnT). Charge perturbations in EDL due to antigen binding resulted in increased capacitance (C_{dl}) which was quantitatively observed as a decrease in impedance with increasing cTnT concentrations as shown in Figure 3A & B. Figure 3B illustrates the changes in phase of measured impedance response. We observe dominant capacitive behavior at low frequencies (<1000 Hz) and resistive behavior at higher frequencies (>10,000 Hz). The frequency at 100 Hz where the maximum impedance change was observed was selected as the optimal frequency for the calibration curve. As these electrochemical studies don't involve any external redox molecule to mediate charge transfer, it is a nonfaradic and hence a label-free biosensing mechanism.

Response to protein interactions in ZnO nanoelectrodes

Mott–Schottky analysis was employed to study the capacitance characteristics ($1/C^2$) of ZnO nanoelectrodes as function of applied potential in the presence of electrolyte with varying concentration of cTnT. Figure 4B & C shows the Mott–Schottky plots between -1 V and +1 V at 0.1 V step and fixed frequency (1000 Hz) for cTnT antigen dose response. Three regions can be clearly distinguished in the Mott–Schottky plots. The region from -1 V to -0.2 V, in other words, the 1st inflexion point corresponds to the capacitance dominated by the space-charge (i.e., C_{SC}). V_{fb} ranged from -1.06 ± 0.11 V with varying concentration of cTnT. With just the PBS (pH~7) and no cTnT concentration V_{fb} is still negatively shifted at -0.9 V compared with that of planar ZnO seed layer -0.42 V as shown in Figure 4C. In

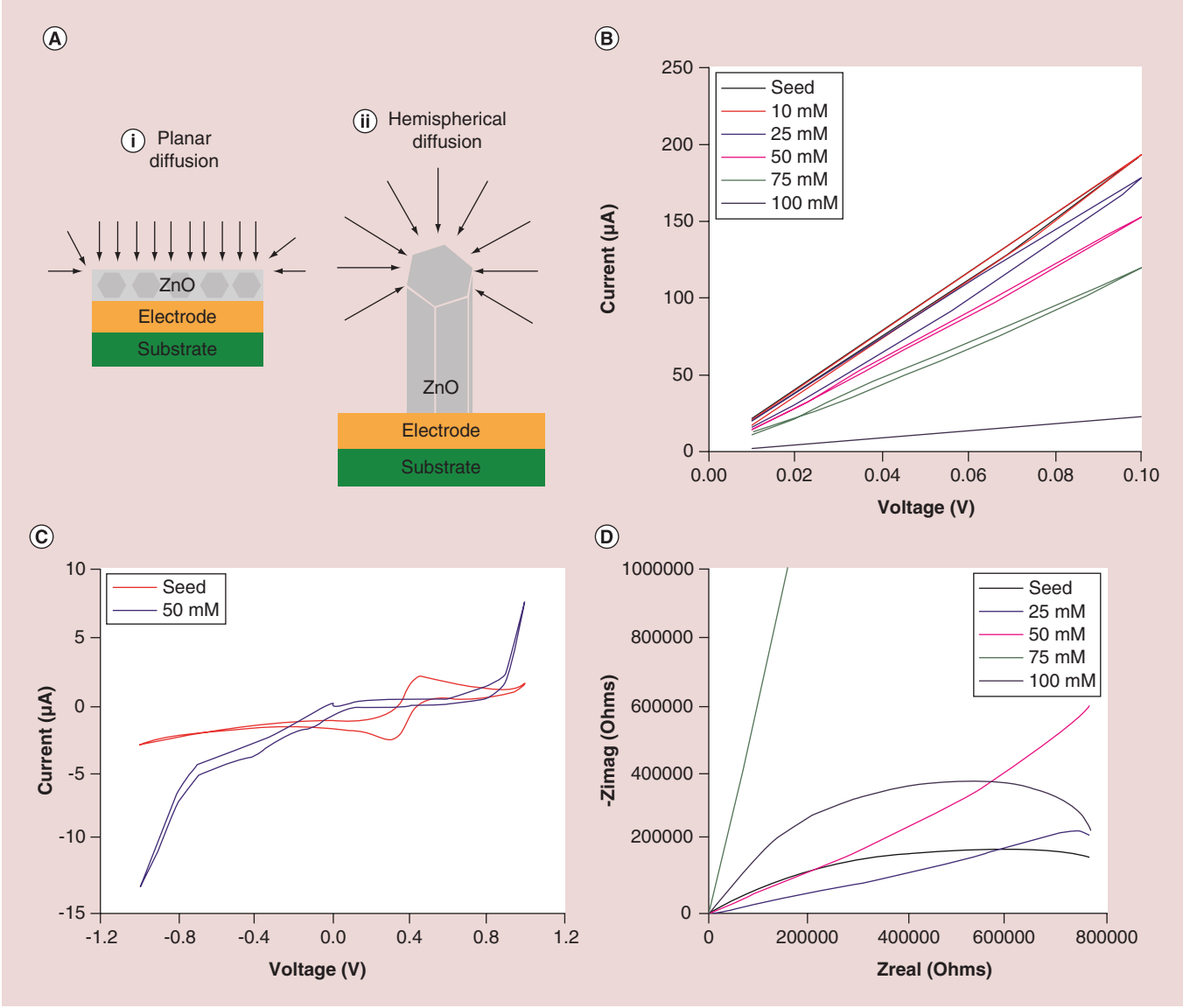

Figure 2. Characterization of ZnO nanostructured electrode behavior. **(A)** Schematic representation of diffusion occurring at planar ZnO electrode and nanostructured ZnO electrode. **(B)** I–V hysteretic curve illustrating the influence of growth density on electrical characteristics of nanostructured electrodes. **(C)** Cyclic voltammogram on seed and 50 mM growth substrate illustrating nanoelectrode behavior in 50 mM precursor concentration growth sensor platform. **(D)** Characteristic impedance spectra observed on nanostructured microelectrode ZnO platform with varying precursor concentration. The deposition conditions for seed layer remained the same across all experiments and data shown here is for tests conducted using PBS buffer medium.

this measurement, copper was the reference electrode with PBS and HS as the electrolyte and based on experiments with respect to both open circuit potential and reference voltage determined the potential of copper reference electrode of +0.52 V. The slope of this linear region also provides an estimate of the carrier density in the semiconductor nanoelectrode. [37,38] Using the equations from these references the donor carrier density value is 3.4–4.8 × 1022 cm^{-3} and the width of space-charge region is altered slightly from 3 to 5.5 nm with increasing concentration of cTnT antigen. At these donor densities, the semiconductor is considered degenerately doped and hence for applied potentials exceeding -0.2 V, the potential drop occurs primarily across the Helmholtz layer and in the bulk electrolyte. The region from -0.2 V to +0.4 V, in other words, the 1st inflexion point to 2nd inflexion point corresponds to the capacitance dominated by the Helmholtz planes, in other words, inner Helmholtz plane (IHP) and outer Helmholtz plane (OHP) that constitute the EDL. Non-linear behavior in Mott–Schottky analysis observed in this region is attributed to the enhancement of the EDL at the interface. Therefore, cTnT antigen binding interactions occurring within EDL are characterized

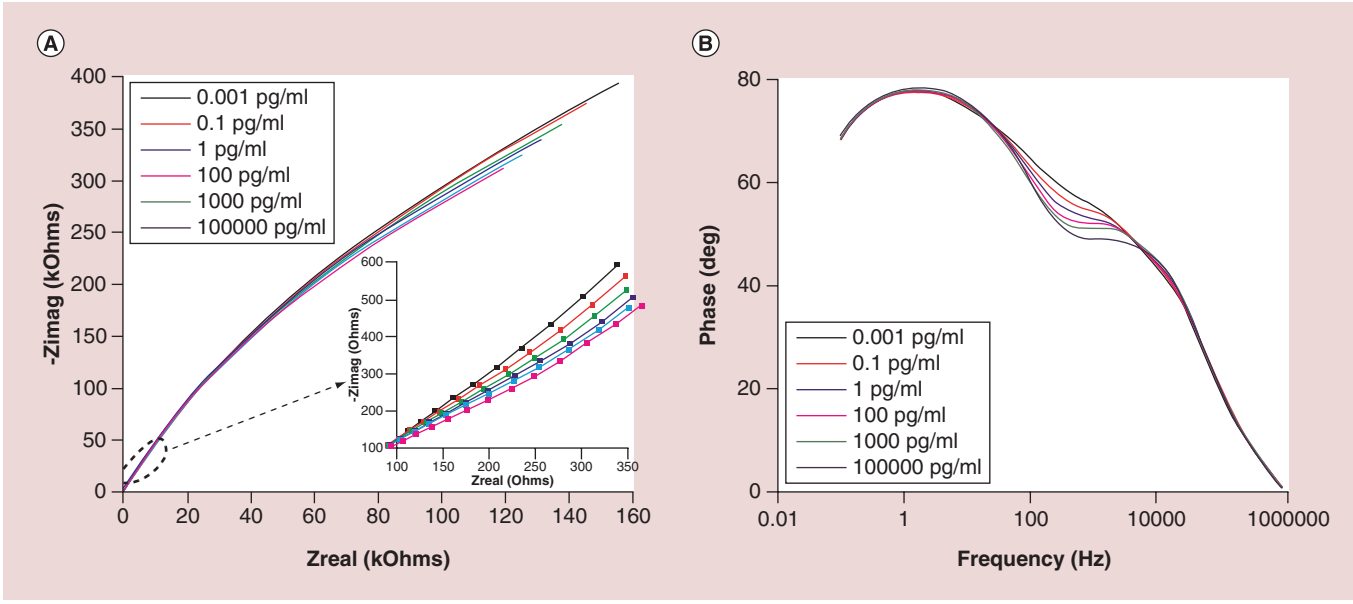

Figure 3. Electrochemical impedance spectroscopy results observed for varying concentrations of cTnT antigen on electrochemical ZnO nanoelectrode sensor platform grown with 50 mM precursor concentration. **(A)** Nyquist plot illustrating decrease in impedance with increasing concentration of cTnT. Inset represents the spread in impedance response for increasing concentrations of cTnT at low frequencies. **(B)** Bode plot representing observed capacitive (<1000 Hz) and resistive (>10,000 Hz) behavior.

within this region and trend with $1/C^2$ decreasing with increasing concentrations of cTnT antigen as shown in Figure 4B & D.

Performance of nanostructured sensing surface for cTnT detection

Sensor calibration dose responses for varying concentrations of cTnT in PBS and HS were built from EIS impedance and Mott–Schottky capacitance measurements to validate this hypothesis. Figure 5A, B & C shows the dose response curve obtained by plotting the percentage change in EIS impedance at 100 Hz and Mott–Schottky capacitance at zero DC bias versus concentration of cTnT respectively for PBS and HS. A correlation of increasing percentage changes, in other words, decrease in measured output signal response from the sensor baseline is found between nonfaradic EIS impedance changes with that of Mott–Schottky capacitance changes over the concentration range of cTnT from 0.001 to 100,000 pg/ml and independent of the buffer media. The LOD in HS was 0.1 pg/ml from both these techniques determined by setting the signal noise threshold for this nanoelectrode electrochemical biosensor at three times the noise signal from EIS impedance (2.5%) and Mott–Schottky capacitance (3.6%), respectively. The dynamic range of percentage change in output signal responses both for the measured EIS impedance associated with changes to C_{dl} as well as for the Mott–Schottky capacitance was about 50%. Control experiments were performed by functionalizing the ZnO nanoelectrodes first with DSP and then blocking the NHS ester terminal groups with Superblock. The response for test concentrations of cTnT is within the established signal noise threshold. This indicates the measured signal response in the calibration experiments are due to interactions between the α-TnT antibody and cTnT antigen. Table 2 summarizes the results of different sensor platforms developed toward detection of cTnT [15,16,39–42].

The capture antibody is prone to interact with other biomolecules in serum-based assays. Thus, specificity of α-cTnT for cTnT detection in serum was established by testing the sensor platforms with different concentrations of BSA prepared in HS. BSA was chosen as albumin is the main protein that constitutes about 55% of total protein concentration in human blood plasma. In addition, BSA has a high tendency to interact with the amine groups which are majorly found on antibody side chains. The maximum change observed with both the techniques was less than 8%, in other words, within the established signal noise threshold. Also the results for cTnT detection in serum were equal to those with neat PBS. These results indicate that the capture antibody shows less cross-reactivity for biomolecules present in HS. Thus, this study has potential clinical relevance in development of electrochemical devices for direct detection of cTnT in serum-based assays.

Discussion

Morphology of ZnO nanostructured sensing surface

At higher concentrations, higher amount of zinc hydroxyl ions are present and results in competitive

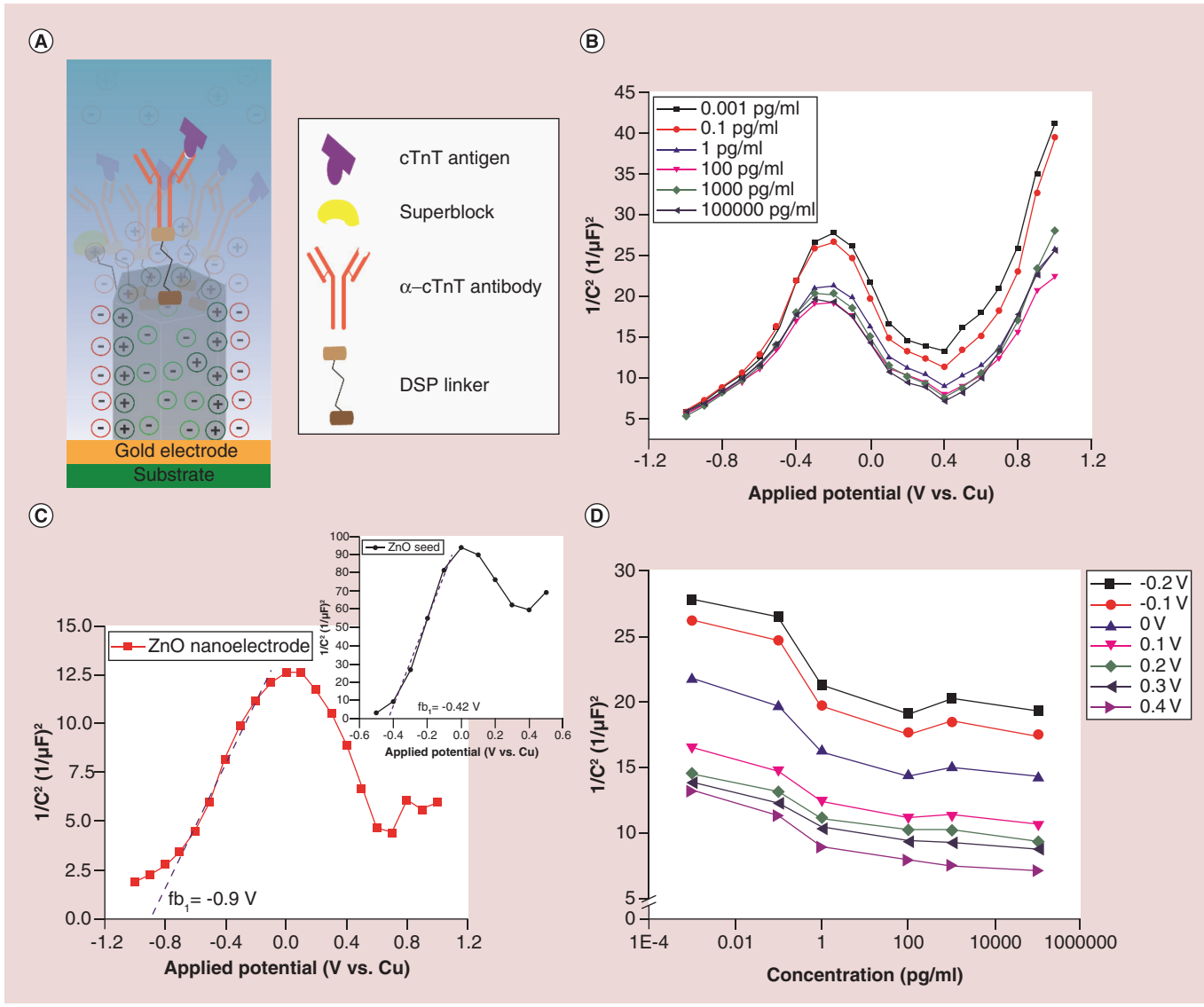

Figure 4. Mott Schottky characterization of protein interactions in ZnO nanoelectrodes. **(A)** Schematic representation of ZnO nanoelectrode/electrolyte interface illustrating biomolecule binding and charge distribution at the interface. **(B)** Mott–Schottky plots showing increasing $1/C^2$ with varying concentrations of cTnT antigen on electrochemical ZnO nanoelectrode sensor platform. **(C)** Mott–Schottky behavior with PBS before cTnT introduction. Inset shows plot for RF-magnetron sputtered ZnO seed substrate in PBS. We observe a negative shift in flatband potential from -0.42 V (ZnO seed) to -0.9 V with ZnO nanoelectrodes. **(D)** Voltage dependency plots for cTnT concentrations and Mott–Schottky capacitance.

binding of these ions at nucleation sites on the seed layer leading to a denser growth. Longer growth times and temperature of bath was also found to influence aspect ratio of nanostructures. Electrochemical biosensor platforms for detection of cTnT were thus synthesized at 80°C for 30 min growth duration that resulted in ZnO nanostructures with aspect ratio ≥4.0. XPS analysis (Supplementary Figure 3) revealed characteristic peaks at 1021.3 eV for Zn 2p and two peaks at 531.8 and 530.1 eV for O 1s confirmed that the synthesized nanostructures are ZnO [43]. Vertically oriented nanostructure arrays with high aspect ratio and spac-

Figure 5. Calibration dose response curve observed on ZnO nanoelectrode sensor platform see facing page). **(A)** Percentage change in EIS impedance with varying cTnT concentrations in PBS and HS. **(B)** Percentage change in Mott–Schottky capacitance for tested concentrations of cTnT. Dotted lines in **(A & B)** represent the control experiments performed in absence of α-cTnT. **(C)** Comparison of output signal response using EIS impedance and Mott–Schottky capacitance for cTnT detection in HS. Dotted lines represent the cross-reactivity of α-cTnT for BSA in HS.
BSA: Bovine serum albumin; EIS: Electrochemical impedance spectroscopy; HS: Human serum.

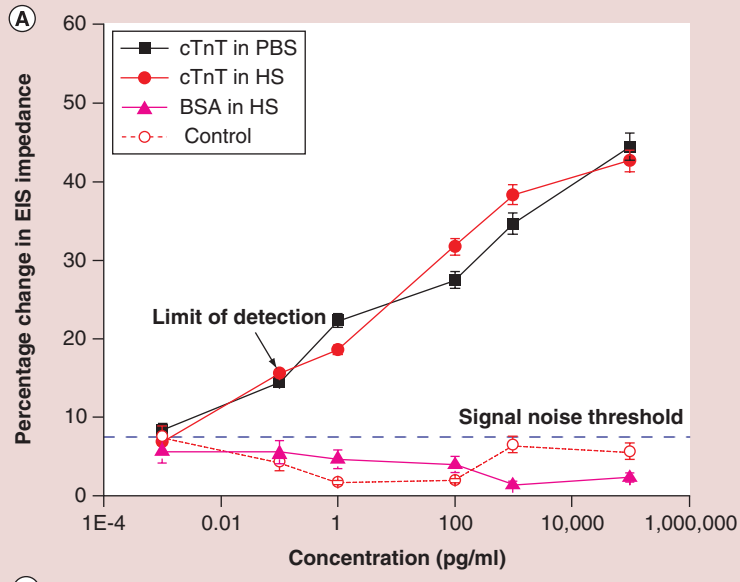
A
Percentage change in EIS impedance
cTnT in PBS
cTnT in HS
BSA in HS
Control
Limit of detection
Signal noise threshold
Concentration (pg/ml)

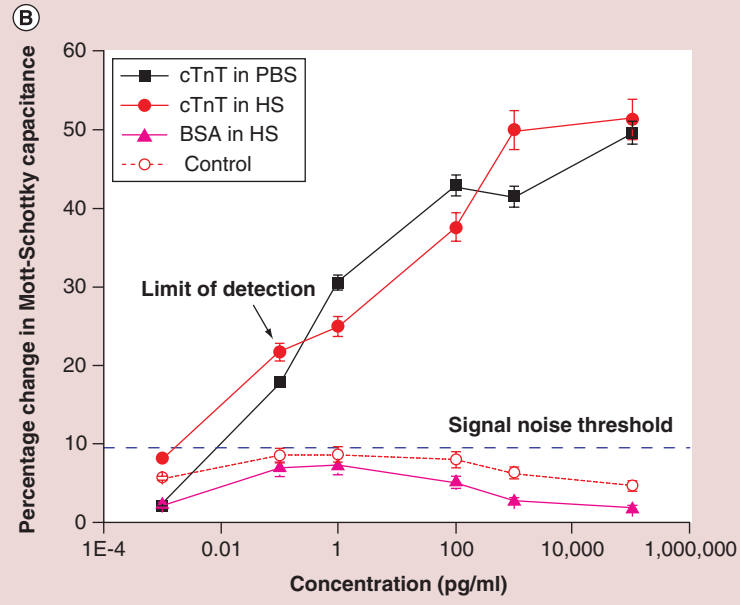
B
Percentage change in Mott-Schottky capacitance
cTnT in PBS
cTnT in HS
BSA in HS
Control
Limit of detection
Signal noise threshold
Concentration (pg/ml)

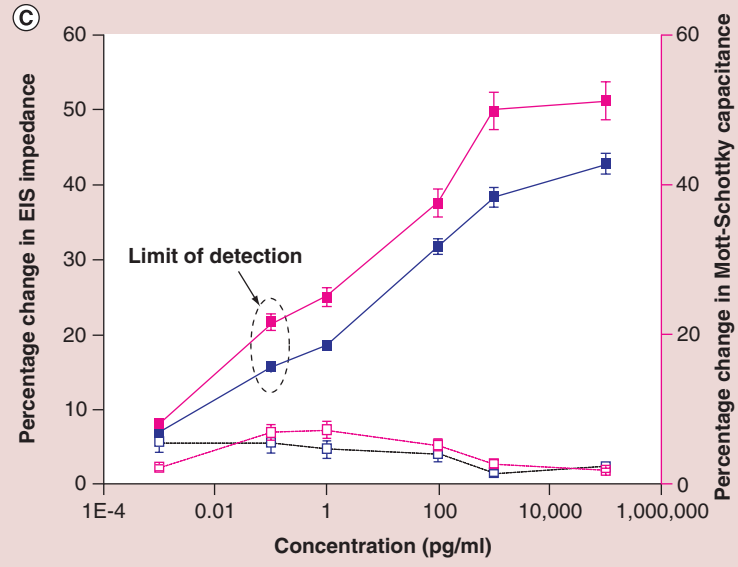
C
Percentage change in EIS impedance
Percentage change in Mott-Schottky capacitance
Limit of detection
Concentration (pg/ml)

ing allowing for electrolyte diffusion enables selective functionalization of biomolecules along the surface of the ZnO nanostructures and influence electrochemical reaction rates and hence the sensitivity of detection.

Investigation of ZnO nanostructured electrode behavior

The electrochemical responses greatly differ at the nanoelectrodes surfaces from the planar electrodes [32,44,45]. The presence of nanoelectrodes facilitate the nonlinear (radial) diffusion with steady-state mass flux to the boundary of the electrode, whereas in planar electrodes the mass transport occurs linearly between the electrode and the bulk solution as shown in Figure 2A. The enhanced mass transport due to increased surface area at the nanoelectrodes results in increased current density and thus signal amplification. A radial diffusion, therefore offers steady-state or near steady state current that allows highly accurate measurements with improved S/Ns as opposed to transient current measurements in planar electrodes. CV response with reversible solution bound redox species at the nanostructured electrodes is sigmoidal shaped with no peaks, whereas the seed electrodes show peaks. The higher measured charge density and the sigmoidal shape of CV curve at nanostructured electrode surfaces in Figure 2C are indicative of the higher surface area and the ZnO nanostructures behaving as capacitive elements facilitating radial diffusion. When the diffusion of molecules to electrode surface occurs within EDL region and without any overlap of EDL's from adjacent nanoelectrodes, nonfaradaic modulations to the charges at the nanostructured electrode/electrolyte interfaces can be characterized with electrochemical analytical methods as described in the following sections. Furthermore, the interspacing distance of the nanoelectrodes should be greater than twice the diffusion distance for radial diffusion to occur at the boundary of the electrode.

Electrochemical characterization of ZnO nanoelectrode/electrolyte interface

Response to protein interactions at EDL formed at the electrolyte interface

EIS in AC steady state was used to monitor the charge perturbations at the ZnO nanoelectrode/electrolyte interface to characterize biomolecular binding. In presence of applied electric field, the ions in the buffer solution are attracted to ZnO nanoelectrode surface resulting in charge distribution gradient at electrode surface and into the electrolyte. The compact layer of ions at electrode surface is the IHP and ionic gradient distribution extending in to electrolyte is the OHP. The OHP is the movable end of EDL that forms innermost layer for diffuse ions and these ions in bulk region contribute to solution resistance (R_{sol}). When DSP is added to the electrode surface, the linker binds to ZnO nanoelectrodes through thiol chemistry [46]. This chemical conjugation displaces OHP resulting in charge perturbations at nanoelectrode surface. This results in change in potential drop between IHP and OHP that can be correlated to C_{dl}. When α-cTnT antibody is added, it binds to other end of DSP linker through biochemical conjugation moving the OHP further away from nanoelectrode. The antigen molecules (cTnT) that bind to antibody immobilized nanoelectrodes further perturb these charge distributions in EDL. Therefore, monitoring the changes in EDL as changes to C_{dl} is indicative of biomolecular binding events and EDL behaves as a dominant capacitive element and bulk solution as resistive element. These interactions are all occurring at the nanoelectrode

Table 2. Comparison of different troponin biosensors based on sensor platform, transduction mechanism and limit of detection reported in the literature.

Sensor platform	Biomarker	Detection technique	Test medium	Concentration range	LOD	Ref.
Silicon nanowire	cTnI	FET – drain current	PBS	0.096–46 ng/ml	0.092 ng/ml	[15]
Nanoporous nylon membrane	cTnT	EIS	Plasma	1E6–1 ng/ml	8.8E6 ng/ml	[16]
Conductive polymer film + carbon nanotubes	cTnT	Cyclic voltammetry	Human serum	0.1–10 ng/ml	0.033 ng/ml	[39]
Gold nanoparticle conjugated detector antibody	cTnT	SPR	Human serum	5–400 ng/ml	0.5 ng/ml	[40]
Liquid crystal + gold nanoparticles	cTnT	Voltammetry + EIS	Human serum	0.1–1 ng/ml	0.076 ng/ml	[41]
Gold electrode + molecularly imprinted polymer	cTnT	Voltammetry	Human serum	0.001–70.3 ng/ml	0.009 ng/ml	[42]
ZnO nanoelectrodes	cTnT	EIS + Mott–Schottky	Human serum	1E6–100 ng/ml	0.0001 ng/ml	

surface and can be measured as impedance changes. This measured impedance has both real and imaginary components contributing to resistive and capacitive components respectively in Randle's equivalent circuit.

Response to protein interactions in ZnO nanoelectrodes

When an n-type semiconductor and a biomolecule complex with surface charge (such as cTnT in contact with α-cTnT) come into contact, where the Fermi level in the semiconductor is higher in energy compared with Fermi level of the electrolyte solution, equilibrium can be achieved through the transfer of electrons from the semiconductor to electrolyte solution so that the Fermi levels for both phases are equal [47]. ZnO nanoelectrodes formed on metallic interconnect and in contact with an electrolyte, in other words, buffer medium is polarized when an external field is applied. This results in electrochemical potential imbalance at ZnO nanoelectrode/electrolyte interface [48,49]. Thus, to maintain thermodynamic equilibrium, an exchange of charges occurs between ZnO nanoelectrodes and electrolyte resulting in localized charge distribution at the interface with positive charge on ZnO side and negative charge on solution side of nanoelectrodes as shown in Figure 4A. The role of the electrode in charge transfer process is important for the accurate characterization and sensing of the biomolecular binding. When a metal electrode comes in contact with an electrolyte, all the potential drop across the interface occurs within the Helmholtz region, in other words, Fermi level is pinned. Unlike in a metal electrode, the potential drop at a semiconductor electrode/electrolyte interface occurs across both in the electrode and the electrolyte. The resulting differential space-charge capacitance (C_{SC}) within the planar semiconductor electrode is much smaller than the differential Helmholtz capacitance (C_H) of the electrolyte [50] and therefore C_H contribution is usually assumed to be negligible in the total capacitance, in other words, band edge is pinned. In contrast for a nanostructured semiconductor electrode/electrolyte interface, C_H is of the same order as that of C_{SC} due to enhancement of EDL and cannot be ignored. The band edge pinning and the Fermi level pinning are the two extreme situations of the potential distribution at the semiconductor/electrolyte interface, and usually the applied potential with respect to the flatband potential (V_{fb}) distributes partly in the space-charge layer and partly in the Helmholtz layer [37].

Performance of nanostructured sensing surface for cTnT detection

Based on Randle's circuit analysis and EIS results, nonfaradaic charge transfer exists in the ZnO nanoelectrode/electrolyte system due to the absence of redox elements. Nonfaradaic electrode capacitance caused by charge build-up at ZnO nanoelectrode surface in the electrolyte is represented by C_{dl} and is a measure of the binding interactions occurring at this interface. This is indicated by the depressed semicircle in the EIS spectra shown in Figure 3A. These binding interactions also modulate the capacitance in the semiconducting ZnO nanoelectrode. Therefore, in such a system C_{dl} measured with EIS complements the capacitance measured with Mott–Schottky analysis and both these methods can effectively be used as detection techniques for ultrasensitive affinity-based biosensing. This indicated in Figure 5 where the dynamic range indicates the nonfaradaic charge build up within the EDL associated with biomolecule affinity-based binding of cTnT antigen on to the antibody immobilized semiconducting ZnO nanoelectrodes. Specificity of charge build up associated with interaction of cTnT with its antibody can be attributed to the corresponding changes to Mott–Schottky capacitance and changes to EIS capacitance. This work is the first experimental demonstration of measuring protein interactions with these combinatorial AC-based EIS and DC-based Mott–Schottky detection techniques and can be extended to other clinically important biomarkers detection. Therefore, this study is highly promising for development of semiconducting metal oxides such as ZnO-based electro analytical devices.

Conclusion

We have demonstrated the tuning of electrical responses of ZnO nanoelectrode sensor platform in an electrolyte medium using a combination of alternating and direct current modulation through the use of EIS and Mott–Schottky techniques, respectively. Using nanoscale dimensions we are able to modulate both C_H and C_{SC} to study the protein biomolecular interactions with varying concentrations within the Helmholtz planes as characterized by the nonlinearity in the Mott–Schottky plot and capacitive behaviors in EIS plot. These experimental results from both these techniques show the tuning of electrical responses is due to the binding interactions occurring within the EDL formed at the ZnO nanoelectrode/electrolyte interfaces and can be effectively used in electrical biosensing applications. We demonstrate the effectiveness of ZnO nanoelectrode sensor platform for electrical biosensing with detection of up to 0.1 pg/ml for cTnT in HS. The response time of the biosensor-defined as the time taken to reach 95% of the signal response was evaluated to be at 10 ms. A strong correlation is established between the Mott–Schottky capacitance in DC mode with EIS impedance in AC mode for

varying concentrations of cTnT and hence both these techniques can be used for designing an ultrasensitive, stable and scalable biosensor devices with the ZnO nanoelectrode sensor platform. Such characterization using a combination of AC and DC methods can be easily extended to other devices consisting of semiconducting nanoelectrodes/electrolyte interfaces that involve EDL tuning for electrical transduction and detection. This combinatorial approach for detection also provides a foundation for development of low-power, multiplexed and ultrasensitive devices for diagnostic and PoC applications.

Future perspective

The zinc oxide nanoelectrode biosensor designed for cTnT sensing has the sensitivity to detect cTnT and potentially distinguish the different isoforms of cTn through the implementation of multiple heights of the nanostructures for achieving size-based screening and controlled diffusion of biomolecules based on size and charge and binding by controlling the diffusion time. The multi geometries of the nanostructures will allow for controlled immobilization of antibodies with specific binding pockets (frequency-based detection at specific heights in the EDL). Ultimately, the key to better diagnosis of AMI is finding more effective ways to use cTnT assay as a screening tool Based on the 99th percentile rule, troponin decision limits of several high-sensitivity cTn assays can be set as low as 0.01 ng/ml [51]. This makes it possible to identify patients with ACS earlier, enabling earlier coronary intervention. However, while improving clinical sensitivity for the diagnosis of myocardial infarction, the increased analytic sensitivity has come at the cost of reduced specificity, thus presenting an additional diagnostic challenge for clinicians. The ZnO nanoelectrode biosensor overcomes the specificity challenges through the combinatorial use of AC and DC spectroscopy. This device demonstrates the potential of designing a rapid PoC test that can be administered in a physician's office and potentially be self-administered for longitudinal monitoring.

Financial & competing interests disclosure

The authors have no relevant affiliations or financial involvement with any organization or entity with a financial interest in or financial conflict with the subject matter or materials discussed in the manuscript. This includes employment, consultancies, honoraria, stock ownership or options, expert testimony, grants or patents received or pending, or royalties.

No writing assistance was utilized in the production of this manuscript.

Supplementary data

To view the supplementary data that accompany this paper please visit the journal website at: www.futuremedicine.com/doi/full/10.2217/nnm-2016-0048

Executive summary

ZnO nanoelectrode biosensor design & fabrication

- Achieves size-based exclusion and controlled binding due to the ZnO nanostructures and the controlled functionalization of biomolecules by leveraging the Zn–S interactions.

Specificity in cTnT detection

- A combinatorial approach involving AC electrochemical impedance spectroscopy and DC Mott–Schottky analysis to characterize dynamic charge transport modulations at the ZnO nanoelectrode/electrolyte interface.
- Detection of cTnT was concurrently achieved through measuring and quantifying the capacitive changes at the interface.

Detection of cTnT in human serum

- LOD of 0.1 pg/ml was achieved in human serum using the combination of AC and DC spectroscopy techniques.

References

Papers of special note have been highlighted as: • of interest; •• of considerable interest

1 Gonzalez SI, La Belle JT. The development of an at-risk biosensor for cardiovascular disease. www.omicsonline.com

2 Pedrero M, Campuzano S, Pingarrón JM. Electrochemical biosensors for the determination of cardiovascular markers: a review. *Electroanalysis* 26(6), 1132–1153 (2014).

3 Buja LM, Entman ML. Modes of myocardial cell injury and cell death in ischemic heart disease. *Circulation* 98(14), 1355–1357 (1998).

4 Daubert MA, Jeremias A. The utility of troponin measurement to detect myocardial infarction: review of the current findings. *Vasc. Health Risk Manag.* 6, 691 (2010).

• **Discusses the role of troponin as a diagnostic and prognostic marker and its assays.**

5 Mcdonnell B, Hearty S, Leonard P, O'Kennedy R. Cardiac biomarkers and the case for point-of-care testing. *Clin. Biochem.* 42(7), 549–561 (2009).

6 Qureshi A, Gurbuz Y, Niazi JH. Biosensors for cardiac biomarkers detection: a review. *Sensors Actuators B Chem.* 171, 62–76 (2012).

7 Lee I, Luo X, Huang J, Cui XT, Yun M. Detection of cardiac biomarkers using single polyaniline nanowire-based conductometric biosensors. *Biosensors* 2(2), 205–220 (2012).

8 Apple FS. Cardiac troponin assays. *Cardiovasc. Toxicol.* 1(2), 93–98 (2001).

9 Sherwood MW, Newby LK. High-sensitivity troponin assays: evidence, indications, and reasonable use. *J. Am. Heart Assoc.* 3(1), e000403 (2014).

10 White HD. Pathobiology of troponin elevations: do elevations occur with myocardial ischemia as well as necrosis? *J. Am. Coll. Cardiol.* 57(24), 2406–2408 (2011).

11 Jarolim P. High sensitivity cardiac troponin assays in the clinical laboratories. *Clin. Chem. Lab. Med.* 53(5), 635–652 (2015).

12 Fang Y. Label-free biosensors for cell biology. *Int. J. Electrochem.* (2011).

13 Mangla A, Gupta S, Staros EB (2015). http://emedicine.medscape.com/article/2087425-overview

14 Chang B-Y, Park S-M. Electrochemical impedance spectroscopy. *Annu. Rev. Analyt. Chem.* 3, 207–229 (2010).

15 Kong T, Su R, Zhang B, Zhang Q, Cheng G. CMOS-compatible, label-free silicon-nanowire biosensors to detect cardiac troponin I for acute myocardial infarction diagnosis. *Biosensors Bioelectron.* 34(1), 267–272 (2012).

16 Barrett TW, Shanmugam NR, Selvam AP, Kazmierczak SC, Prasad S. Novel nanomonitor ultra-sensitive detection of troponin T. *Clin. Chim. Acta* 442, 96–101 (2015).

17 Yakimova R, Selegård L, Khranovskyy V, Pearce R, Lloyd Spetz A, Uvdal K. ZnO materials and surface tailoring for biosensing. *Front. Biosci.* 4(1), 254–278 (2012).

- **Summarizes the preparation techniques, properties and surface modifications that are of considerable interest in design of sensor described in our manuscript.**

18 Devan RS, Patil RA, Lin JH, Ma YR. One-dimensional metal-oxide nanostructures: recent developments in synthesis, characterization, and applications. *Adv. Funct. Mater.* 22(16), 3326–3370 (2012).

19 Willander M, Khun K, Ibupoto ZH. Metal oxide nanosensors using polymeric membranes, enzymes and antibody receptors as ion and molecular recognition elements. *Sensors* 14(5), 8605–8632 (2014).

20 Vayssieres L. Growth of arrayed nanorods and nanowires of ZnO from aqueous solutions. *Adv. Mater.* 15(5), 464–466 (2003).

21 Wang ZL. Zinc oxide nanostructures: growth, properties and applications. *J. Phys.* 16(25), R829 (2004).

22 Korotcenkov G. Metal oxides for solid-state gas sensors: what determines our choice? *Mater. Sci. Eng. B* 139(1), 1–23 (2007).

23 Asif MH, Elinder F, Willander M. Electrochemical biosensors based on ZnO nanostructures to measure intracellular metal ions and glucose. *J. Anal. Bioanal. Tech.* S7, 003 (2011).

24 Chen P-C, Shen G, Zhou C. Chemical sensors and electronic noses based on 1-D metal oxide nanostructures. *Nanotechnol. IEEE Transact.* 7(6), 668–682 (2008).

25 Xu S, Wang ZL. One-dimensional ZnO nanostructures: solution growth and functional properties. *Nano Res.* 4(11), 1013–1098 (2011).

26 Balasubramanian K. Challenges in the use of 1D nanostructures for on-chip biosensing and diagnostics: a review. *Biosensors Bioelectron.* 26(4), 1195–1204 (2010).

27 Maehashi K, Katsura T, Kerman K, Takamura Y, Matsumoto K, Tamiya E. Label-free protein biosensor based on aptamer-modified carbon nanotube field-effect transistors. *Anal. Chem.* 79(2), 782–787 (2007).

28 Feigel IM, Vedala H, Star A. Biosensors based on one-dimensional nanostructures. *J. Mater. Chem.* 21(25), 8940–8954 (2011).

29 Choi A, Kim K, Jung H-I, Lee SY. ZnO nanowire biosensors for detection of biomolecular interactions in enhancement mode. *Sensors Actuators B Chem.* 148(2), 577–582 (2010).

30 Munje RD, Jacobs M, Muthukumar S, Quadri B, Shanmugam NR, Prasad S. A novel approach for electrical tuning of nano-textured zinc oxide surfaces for ultra-sensitive troponin-T detection. *Anal. Methods* 7(24), 10136–10144 (2015).

31 Bogomolova A, Komarova E, Reber K *et al.* Challenges of electrochemical impedance spectroscopy in protein biosensing. *Anal. Chem.* 81(10), 3944–3949 (2009).

- **Challenges in designing label-free impedance biosensors has been detailed in this manuscript.**

32 Arrigan DW. Nanoelectrodes, nanoelectrode arrays and their applications. *Analyst* 129(12), 1157–1165 (2004).

33 Jacobs M, Muthukumar S, Selvam AP, Craven JE, Prasad S. Ultra-sensitive electrical immunoassay biosensors using nanotextured zinc oxide thin films on printed circuit board platforms. *Biosensors Bioelectron.* 55, 7–13 (2014).

34 Baruah S, Dutta J. Hydrothermal growth of ZnO nanostructures. *Sci. Technol. Adv. Mater.* 10(1), 013001 (2009).

35 Amin G, Asif M, Zainelabdin A, Zaman S, Nur O, Willander M. Influence of pH, precursor concentration, growth time, and temperature on the morphology of ZnO nanostructures grown by the hydrothermal method. *J. Nanomater.* 2011, 5 (2011).

- **Outlines the influence of hydrothermal growth parameters on ZnO nanostructure formation and issues related to it.**

36 Polsongkram D, Chamninok P, Pukird S *et al.* Effect of synthesis conditions on the growth of ZnO nanorods via hydrothermal method. *Physica B* 403(19), 3713–3717 (2008).

37 Uosaki K, Kita H. Effects of the Helmholtz layer capacitance on the potential distribution at semiconductor/electrolyte interface and the linearity of the Mott–Schottky plot. *J. Electrochem. Soc.* 130(4), 895–897 (1983).

- **The distribution of charges at the semiconductor electrode/electrolyte interface is crucial for capacitive based measurements.**

38 Mora-Seró I, Fabregat-Santiago F, Denier B *et al.* Determination of carrier density of ZnO nanowires by electrochemical techniques. *Appl. Phys. Lett.* 89(20), 203117 (2006).

39 Gomes-Filho S, Dias A, Silva M, Silva B, Dutra R. A carbon nanotube-based electrochemical immunosensor for cardiac troponin T. *Microchem. J.* 109, 10–15 (2013).

40 Pawula M, Altintas Z, Tothill IE. SPR detection of cardiac troponin T for acute myocardial infarction. *Talanta* 146, 823–830 (2016).

41 Zapp E, Da Silva PSR, Westphal E, Gallardo H, Spinelli A, Vieira IC. Troponin T immunosensor based on liquid crystal and silsesquioxane-supported gold nanoparticles. *Bioconj. Chem.* 25(9), 1638–1643 (2014).

42 Karimian N, Vagin M, Zavar MHA, Chamsaz M, Turner APF, Tiwari A. An ultrasensitive molecularly-imprinted human cardiac troponin sensor. *Biosensors Bioelectron.* 50, 492–498 (2013).

43 Al-Gaashani R, Radiman S, Daud AR, Tabet N, Al-Douri Y. XPS and optical studies of different morphologies of ZnO nanostructures prepared by microwave methods. *Ceram. Int.* 39(3), 2283–2292 (2013).

44 Aoki K. Theory of ultramicroelectrodes. *Electroanalysis* 5(8), 627–639 (1993).

45 Stulík K, Amatore C, Holub K, Marecek V, Kutner W. Microelectrodes. Definitions, characterization, and applications (Technical report). *Pure Appl. Chem.* 72(8), 1483–1492 (2000).

46 Chen J, Ruther RE, Tan Y, Bishop LM, Hamers RJ. Molecular adsorption on ZnO ($10\bar{1}0$) single-crystal surfaces: morphology and charge transfer. *Langmuir* 28(28), 10437–10445 (2012).

47 Gelderman K, Lee L, Donne S. Flat-band potential of a semiconductor: using the Mott–Schottky equation. *J. Chem. Educ.* 84(4), 685 (2007).

48 Al-Hilli S, Willander M. The pH response and sensing mechanism of n-type ZnO/electrolyte interfaces. *Sensors* 9(9), 7445–7480 (2009).

49 Rajeshwar K. Fundamentals of semiconductor electrochemistry and photoelectrochemistry. In: *Encyclopedia Of Electrochemistry*. Wiley (2002).

50 Morrison SR. *Electrochemistry At Semiconductor And Oxidized Metal Electrodes*. Plenum Press, NY, USA (1980).

51 Apple FS, Parvin CA, Buechler KF, Christenson RH, Wu AH, Jaffe AS. Validation of the 99th percentile cutoff independent of assay imprecision (CV) for cardiac troponin monitoring for ruling out myocardial infarction. *Clin. Chem.* 51(11), 2198–2200 (2005).